Simulation of the Mode Dynamics in Broad-Ridge Laser Diodes

Eduard Kuhn

***Abstract*—In this publication a new approach to simulate the mode dynamics in broad-ridge laser diode is presented. These devices exhibit rich lateral mode dynamics in addition to longitudinal mode dynamics observed in narrow-ridge laser diodes. The mode dynamics are strongly influenced by higher order effects, which are described by effective interaction terms and can derived from the band structure and the carrier scattering in the quantum well. The spatial dependency of pump current densities plays a crucial role in lateral mode dynamics, and thus, a Drift-Diffusion model is employed to calculate the current densities with an additional capturing term.**

***Index Terms*—Laser diode, mode dynamics, gallium nitride, nitride laser diode, mode competition.**

I. Introduction

FABRY-PÉROT type laser diodes find use in a diverse range of applications such as laser displays [1], [2], [3], [4] and projection [5], [6], [7], exhibiting phenomena related to mode competition [8], [9]. These lasers often demonstrate mode hopping, wherein the relative activity levels of different longitudinal modes change with respect to time due to an antisymmetric interaction among these modes. In a recent development, a similar effect has been noted in broad area laser diodes, where multiple lateral modes are present [10]. This mode interaction can be explained by the beating vibrations of carrier densities within the quantum well, which appear when several longitudinal modes are concurrently active [11].

The most common approach for simulating mode dynamics in these devices involves using rate equations, which entail formulating equations of motion for the photon numbers of the different optical modes and the quantum well carrier densities. An alternative method, the traveling wave method, involves solving a partial differential equation for the electrical field [12], [13], [14], [15], [16], [17], [18]. Nonetheless, thus far, simulations of mode dynamics using the traveling wave method have not succeeded in reproducing the experimental results.

As the mode dynamics are strongly influenced by higher order effects such as beating vibrations of the carrier densities or spectral hole burning, it is insufficient to consider a spatially constant carrier density in the rate equations. One possibility is to use spatial and energy-dependent distribution functions [19], but these calculations are very computationally expensive. Alternatively it is possible to add an effective mode interaction term to the rate equations for the photon numbers, which has been initially derived for maser devices by Lamb et al. [20]. In literature this term can be found for single lateral mode Fabry-Pérot laser diodes [11], [21], [22], [23], [24], [25] and also for devices with multiple lateral modes [26].

Another important aspect for the simulation of Fabry-Pérot laser diodes with multiple lateral modes is the spatial dependency of the pump current densities. A higher current density in a specific area can result in an increased carrier density, leading to higher optical gain. Consequently, the modal gain of lateral modes increases when their mode functions reach a maximum in that region. Thus, it is important to accurately describe these pump current distributions in order to describe the lateral mode dynamics. For this purpose the Drift-Diffusion equations are often used in literature to describe carrier transport and to study the properties of semiconductor laser devices [27], [28], [29], [30], [31].

In this paper a new method is presented, where the rate equations with an effective mode interaction term are combined with an improved description of carrier transport using the Drift-Diffusion equations. As the time scale of the mode dynamics is in the region of $100\,\mathrm{ns}$, using a time-dependent Drift-Diffusion model would be too computationally expensive. Thus the Drift-Diffusion equations are solved for a steady state. The resulting pump current densities are used in a subsequent mode dynamics simulation, where only the carriers in the quantum wells are considered in the dynamic equations. In Section III simulation results using this method for a green nitride laser diode with a ridge width of $10\,\mu\mathrm{m}$.

II. Theory

A. Mode Function

The goal of this publication is the simulation of the mode dynamics in Fabry-Pérot type laser diodes. For this purpose the optical field is expanded using mode functions:

$$\mathbf{E}(\mathbf{r}) = \sum_{mp} i\sqrt{\frac{\hbar\omega_{mp}}{2\epsilon_0}}\left[B_{mp}\mathbf{u}_{mp}(\mathbf{r}) - B^*_{mp}\mathbf{u}^*_{mp}(\mathbf{r})\right], \quad (1)$$

where ϵ_0 is the vacuum permittivity, ω_{mp} is the angular frequency of the mode with indices mp, B_{mp} is the respective mode coefficient and $\mathbf{u}_{mp}(\mathbf{r})$ is the mode function. The goal of the mode dynamics simulation is to know how mode coefficients

Manuscript received 1 December 2023; revised 15 February 2024; accepted 5 March 2024. Date of publication 7 March 2024; date of current version 8 April 2024. This work was performed in the frame of the Leibniz-Gemeinschaft funded project "PCSELence" (Grant No. K487/2022).

The author is with the Weierstrass Institute for Applied Analysis and Stochastics, 10117 Berlin, Germany (e-mail: kuhn@wias-berlin.de).

Digital Object Identifier 10.1109/JPHOT.2024.3374448

B_{mp} or the number of photons in each mode $S_{mp} = |B_{mp}|^2$ change with respect to time. It is assumed that the ridge width of the laser diode is small compared to the resonator length in order to be able to separate the longitudinal and transverse contributions of the mode functions $\mathbf{u}_{mp}(\mathbf{r}_\parallel, z)$:

$$\mathbf{u}_{mp}(\mathbf{r}) = \mathbf{t}_m(x,z) g_p(y).$$

Here the index m is used to number the transverse modes $\mathbf{t}_m$ and p the longitudinal modes g_p. The coordinates are chosen so that the optical field propagates in y direction and the device is grown in z direction. For transverse electric (TE) modes the polarization primarily points in the x direction $\mathbf{t}_m(x,z) = \mathbf{e}_x t_m(x,z)$ and the transverse modes are given by the eigen equation [32]

$$\left(\frac{\partial^2}{\partial x^2} + \frac{\partial^2}{\partial z^2}\right) t_m(x,z) + \frac{\omega^2}{c^2} n^2(x,z,\omega) t_m(x,z) = \frac{\omega^2}{c^2} \left(n^m_{\text{eff}}(\omega)\right)^2 t_m(x,z) \tag{2}$$

for a given refractive index profile $n(x,z,\omega)$ and the interface conditions for the electromagnetic field. In the simulations this equation is solved for a frequency ω_0 near the gain maximum in order to obtain the transverse mode functions $t_m(x,z)$, their respective effective refractive indices $n^m_{\text{eff}}(\omega_0)$ and the group refractive indices

$$n^m_{\text{gr}}(\omega_0) = n^m_{\text{eff}}(\omega_0) + \omega_0 \frac{\partial n^m_{\text{eff}}(\omega_0)}{\partial \omega_0}.$$

The group refractive index determines the longitudinal mode spacing and is used to calculate the mode frequencies

$$\omega_{mp} = \frac{\pi c}{n^m_{\text{eff}}(\omega_0) L} p_0 + \frac{\pi c}{n^m_{\text{gr}}(\omega_0) L} \left(p - p^m_0\right), \quad \text{where} \quad p^m_0 = \text{round}\left(\frac{n^m_{\text{eff}}(\omega_0) L \omega_0}{\pi c}\right) \tag{3}$$

and L is the resonator length. The normalization of the mode functions is given by [33]

$$\int \mathrm{d}x \int \mathrm{d}z\, n^2(x,z,\omega) \left|t_m(x,z)\right|^2 = 1,$$

so that the photon numbers are given by the absolute squares of the expansion coefficients B_{mp} in (1).

B. Mode Dynamics

The equations of motion for the carriers and photon numbers can be derived in the Heisenberg picture [33] and for the carrier densities n_{e} and n_{h} are approximately given by [26]

$$\begin{aligned}\frac{\mathrm{d}}{\mathrm{d}t} n_{\text{e,h}}(x) = &- B\left(n_{\text{e}}(x), n_{\text{h}}(x)\right) - \frac{n_{\text{e,h}}(x)}{\tau_{\text{nr}}} \\ &+ D_{\text{e,h}} \frac{\partial^2}{\partial x^2} n_{\text{e,h}}(x) + \left.\frac{\mathrm{d}}{\mathrm{d}t} n_{\text{e,h}}(x)\right|_{\text{Pump}} \\ &+ \sum_{mp} \left|t_m(x, z_{\text{QW}})\right|^2 \omega_{mp} \frac{S_{mp}}{L} \\ &\times \operatorname{Im} \chi\left(\omega_{mp}, n_{\text{e}}(x), n_{\text{h}}(x)\right).\end{aligned} \tag{4}$$

The first two terms describe the losses due to spontaneous emission and nonradiative processes. The next two terms are used to describe the pumping and diffusion of carriers inside the quantum wells, while the last term gives the losses due to stimulated emission. The stimulated emission term is proportional to the photon numbers S_{mp} and the imaginary part of the susceptibility $\operatorname{Im}\chi$ is evaluated at the respective mode frequencies. The losses due to spontaneous emission $B(n_{\text{e}}, n_{\text{h}})$ and the susceptibility $\chi(\omega, n_{\text{e}}, n_{\text{h}})$ depend on the carrier densities and are calculated using Fermi-Dirac distributions with a fixed temperature. The equations of motion for the photon numbers are given by [26], [33]

$$\begin{aligned}\frac{\mathrm{d}}{\mathrm{d}t} S_{mp} = &- \omega_{mp} S_{mp} \int \mathrm{d}x\, \left|t_m(x, z_{\text{QW}})\right|^2 \operatorname{Im} \chi\left(\omega_{mp}, n_{\text{e}}, n_{\text{h}}\right) \\ &+ \int \mathrm{d}x\, \left|t_m(x, z_{\text{QW}})\right|^2 I_{\text{SE}}\left(\omega_{mp}, n_{\text{e}}, n_{\text{h}}\right) \\ &- \frac{S_{mp}}{\tau_{\text{photon}}} + \left.\frac{\mathrm{d}}{\mathrm{d}t} S_{mp}\right|_{\text{Interaction}}.\end{aligned} \tag{5}$$

The first three term denote changes of the photon numbers due to stimulated emission, spontaneous emission and losses respectively. The last term is used to describe an effective interaction between the optical modes due to third order effects. Without this last term there would be no mode competition effects and in a simulation a steady state would be reached after a few nano seconds, where only the longitudinal mode with the highest gain would be active. The effective mode interaction is derived in [26] and is given by sum over all the other transverse and longitudinal modes:

$$\begin{aligned}\left.\frac{\mathrm{d}}{\mathrm{d}t} S_{mp}\right|_{\text{Interaction}} \approx &\sum_{nq} \frac{1}{2L} \frac{S_{mp} S_{nq}}{\omega_{mp} \omega_{nq}} \\ &\times \int \mathrm{d}x\, \left|t_m(x, z_{\text{QW}})\right|^2 \left|t_n(x, z_{\text{QW}})\right|^2 \\ &\times G\left(\omega_{nq} - \omega_{mp}, n_{\text{e}}(x), n_{\text{h}}(x)\right).\end{aligned} \tag{6}$$

Here the mode interaction between two modes is proportional to their corresponding photon numbers S_{mp} and an integral of the absolute squares of their respective transverse mode function at the position of the quantum well $|t_m x, z_{\text{QW}}|^2$ multiplied with a function $G(\Delta\omega, n_{\text{e}}, n_{\text{h}})$. This function determines the strength of the mode interaction and depends on the frequency difference $\omega_{nq} - \omega_{mp}$ and quantum well properties such as the carrier densities.

A change of the carrier densities causes the susceptibility of the quantum wells to change. The resulting perturbations of the mode functions can also be included in the calculations by solving the one-dimensional Eigen equation [34]

$$\frac{\partial^2}{\partial x^2} \tilde{t}_m(x) + k_0^2 \epsilon_{1\text{D}}(x) \tilde{t}_m(x) = k_0^2 n^2_{\text{eff},m} \tilde{t}_m(x), \tag{7}$$

where $\tilde{t}_m$ is the corrected transverse mode function at the position of the quantum well and $n_{\text{eff},m}$ is the corrected refractive

index. The effective dielectric function is given by

$$\epsilon_{\mathrm{1D}}(x) = \frac{\int \mathrm{d}z\ |t_0(x,z)|^2\, n^2(\omega_0,x,z)}{\int \mathrm{d}z\ |t_0(x,z)|^2} + \delta\epsilon(x) \int_{\mathrm{QW}} \mathrm{d}x\,\mathrm{d}z\ |t_0(x,z)|^2$$

where $t_0(x,z)$ is the solution of the two-dimensional Eigen equation (2) and $n^2(\omega_0,x,z)$ is the respective refractive index profile. The change of the dielectric function in the quantum well is given by

$$\delta\epsilon(x) = \frac{1}{d_{\mathrm{QW}}}\left[\chi\left(\omega_0, n_{\mathrm{e}}(x), n_{\mathrm{h}}(x)\right) - \chi\left(\omega_0, n_{\mathrm{e}}^{\mathrm{ref}}, n_{\mathrm{h}}^{\mathrm{ref}}\right)\right],$$

where the reference densities $n_{\mathrm{e}}^{\mathrm{ref}}$ and $n_{\mathrm{h}}^{\mathrm{ref}}$ are included in the two-dimensional Eigen equation and are chosen close to the threshold densities.

It is possible to solve the equations of motion for a given pump term, for example a constant pump current density:

$$\frac{\mathrm{d}}{\mathrm{d}t} n_{\mathrm{e,h}}(x)\bigg|_{\mathrm{Pump}} = j_0.$$

For laser diodes with larger ridge widths multiple transverse modes participate in the mode dynamics. For an accurate simulation of the mode dynamics it is therefore important to know the spatial dependency of the pump term, in order to estimate which transverse modes benefit based on their respective lateral mode profiles. For example, if the pump term has a global maximum at a certain point then transverse modes will be important when their respective mode functions also have a maximum near that point.

C. Drift-Diffusion Model

For a more detailed calculation of the pump term we perform a steady state calculation, where the carriers in the bulk material are treated separately from the carriers in the quantum wells. For the bulk carriers we use use the Drift-Diffusion equations which are given by [35], [36]

$$\begin{aligned} -\nabla\left(\frac{\mu_{\mathrm{e}}^{\mathrm{M}}}{e} n_{\mathrm{e}}^{\mathrm{3D}} \nabla\mu_{\mathrm{e}}\right) &= R_{\mathrm{e}}(n_{\mathrm{e}}^{\mathrm{3D}}, n_{\mathrm{h}}^{\mathrm{3D}}, \phi) \\ -\nabla\left(\frac{\mu_{\mathrm{h}}^{\mathrm{M}}}{e} n_{\mathrm{h}}^{\mathrm{3D}} \nabla\mu_{\mathrm{h}}\right) &= R_{\mathrm{h}}(n_{\mathrm{e}}^{\mathrm{3D}}, n_{\mathrm{h}}^{\mathrm{3D}}, \phi) \\ -\nabla\left(\epsilon_0\epsilon_r\nabla\phi\right) = \rho &= e\left(n_{\mathrm{h}}^{\mathrm{3D}} - n_{\mathrm{e}}^{\mathrm{3D}} + C\right) + \rho_{\mathrm{QW}}, \end{aligned} \quad (8)$$

where $\mu_{\mathrm{e,h}}^{\mathrm{M}}$ are the mobilities, $\mu_{\mathrm{e,h}}$ are the chemical potentials, ϕ is the static electrical field and C is the charge density due to doping. The relationship between the bulk densities n^{3D} and the chemical potentials is given by the Boltzmann distribution as shown in [35], but is possible to use other statistical functions [27], [28].

The equations for quantum well carriers and the photon numbers are given by (4) and (5) where the time derivatives are set to zero. There are no mode dynamics in the steady state calculation, therefore it is sufficient to only consider one longitudinal mode per transverse mode, here the mode with the frequency closest to the gain maximum ω_0 is used. The charge density of the quantum well carriers is included in poisson equation as an additional charge density:

$$\rho_{\mathrm{QW}} = \begin{cases} \frac{e}{d_{\mathrm{QW}}}\left(n_{\mathrm{h}} - n_{\mathrm{e}}\right) & \text{for } |z - z_{\mathrm{QW}}| < \frac{d_{\mathrm{QW}}}{2} \\ 0 & \text{elsewhere} \end{cases},$$

where d_{QW} is the quantum well thickness. The capture of the bulk carriers into the quantum wells is included in the recombination term:

$$\begin{aligned} R_{\mathrm{e,h}} = R_{\mathrm{e,h}}^{\mathrm{capture}} &- n_{\mathrm{e}}^{\mathrm{3D}} n_{\mathrm{h}}^{\mathrm{3D}} \left(1 - \mathrm{e}^{\beta(\mu_{\mathrm{e}}+\mu_{\mathrm{h}})}\right) \\ &\times \left(\frac{1}{\tau_{\mathrm{e}}\left(n_{\mathrm{e}}^{\mathrm{3D}} + n_{\mathrm{e}}^{0}\right)} + \frac{1}{\tau_{\mathrm{h}}\left(n_{\mathrm{h}}^{\mathrm{3D}} + n_{\mathrm{h}}^{0}\right)}\right. \\ &\left. + c_{\mathrm{e}} n_{\mathrm{e}}^{\mathrm{3D}} + c_{\mathrm{h}} n_{\mathrm{h}}^{\mathrm{3D}} + r_{\mathrm{spont}}\right), \end{aligned}$$

where the second term describes the losses due to spontaneous emission, SRH and Auger recombination [35]. The capture term is only considered for $|z - z_{\mathrm{QW}}| < d_{\mathrm{QW}}/2$, and is given by

$$R_{\mathrm{e,h}}^{\mathrm{capture}} = C_{\mathrm{e,h}} n_{\mathrm{e,h}} \eta_{\mathrm{e,h}}\left(n_{\mathrm{e,h}}, n_{\mathrm{e,h}}^{\mathrm{3D}}\right).$$

The constants $C_{\mathrm{e,h}}$ determine the strength of the capture process and the efficiencies $\eta_{\mathrm{e,h}}$ are given by

$$\eta\left(n, n^{\mathrm{3D}}\right) = \frac{\sum_{\mathbf{k},k_z} f_{\mathbf{k},k_z}^{\mathrm{Bulk}}\left(1 - f_{\mathbf{k}}\right)}{\sum_{\mathbf{k},k_z} f_{\mathbf{k},k_z}^{\mathrm{Bulk}}},$$

where both $f_{\mathbf{k},k_z}^{\mathrm{Bulk}}$ and $f_{\mathbf{k}}$ are Fermi-Dirac distributions that reproduce the densities n and n^{3D} for a fixed temperature. Similar capture terms can be found in literature [31], [37]. For the bulk carriers the $\mathbf{k}\cdot\mathbf{p}$ method is used to calculate the three-dimensional band structure using the parameters from the material surrounding the quantum well. For the carriers in the quantum well the $\mathbf{k}\cdot\mathbf{p}$ method is used as well, here a one-dimensional differential equation is solved in order to obtain the two-dimensional band structure.

The pump term in (4) is then given by

$$\frac{\mathrm{d}}{\mathrm{d}t} n_{\mathrm{e,h}}\bigg|_{\mathrm{Pump}} = C_{\mathrm{e,h}} \int_{\mathrm{QW}} \mathrm{d}z\, n_{\mathrm{e,h}}^{\mathrm{3D}} \eta_{\mathrm{e,h}}\left(n_{\mathrm{e,h}}, n_{\mathrm{e,h}}^{\mathrm{3D}}\right) = j_{\mathrm{e,h}}^{0}. \quad (9)$$

This way the equilibrium current densities can be calculated for every voltage and can be included in the dynamic simulations. However, in order to include changes of the pump current densities due to changes of the quantum well densities in the dynamic simulations, the equation

$$C_{\mathrm{e,h}} d_{\mathrm{QW}} n_{\mathrm{e,h}}^{\mathrm{3D,0}} \eta_{\mathrm{e,h}}\left(n_{\mathrm{e,h}}, n_{\mathrm{e,h}}^{\mathrm{3D,0}}\right) = j_{\mathrm{e,h}}^{0},$$

is solved for an effective three-dimensional density $n_{\mathrm{e,h}}^{\mathrm{3D,0}}$ using the two-dimensional density and the current density from the equilibrium simulation. The pump term in (4) is then given by

$$\frac{\mathrm{d}}{\mathrm{d}t} n_{\mathrm{e,h}}\bigg|_{\mathrm{Pump}} = C_{\mathrm{e,h}} d_{\mathrm{QW}} n_{\mathrm{e,h}}^{\mathrm{3D,0}} \eta_{\mathrm{e,h}}\left(n_{\mathrm{e,h}}, n_{\mathrm{e,h}}^{\mathrm{3D,0}}\right).$$

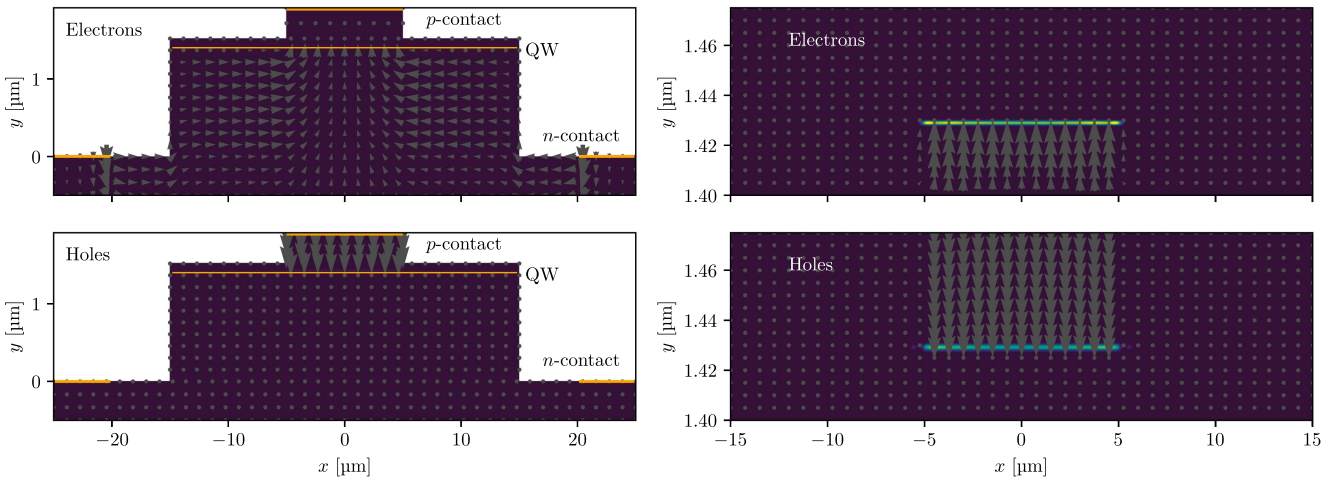

Fig. 1. Solution of the stationary Drift-Diffusion model for a single QW laser diode with a ridge width of $10\,\mu$m and a voltage of $4\,$V. The arrows denote the carrier current densities for electrons and holes, while the colors indicate the recombination term. On the right side the region near the quantum well is shown in more detail. The positions of the quantum well and the contacts are indicated in orange.

TABLE I
REMAINING SIMULATION PARAMETERS

L	cavity length	$600\,\mu$m
T	carrier temperature	$300\,$K
τ_s	scattering time	$300\,$fs
γ	dephasing constant	$30\,$meV
τ_nr	nonradiative losses (QW)	$5\,$ns
τ_photon	photon lifetime	$5.9\,$ps
D_e	electron diffusion constant (QW)	$151.9\,\mathrm{nm^2 ps^{-1}}$
D_h	hole diffusion constant (QW)	$7.77\,\mathrm{nm^2 ps^{-1}}$
C_e	electron capture constant	$1\,\mathrm{ps^{-1}}$
C_h	hole capture constant	$100\,\mathrm{ps^{-1}}$
τ_e	electron nonradiative losses	$1\,$ns
τ_h	hole nonradiative losses	$1\,$ns
r_spont	bulk spontaneous emission losses	$0.01\,\mathrm{nm^3 ps^{-1}}$
c_e	electron Auger losses	$0.01\,\mathrm{nm^6 ps^{-1}}$
c_h	hole Auger losses	$0.01\,\mathrm{nm^6 ps^{-1}}$
n_e^0	electron density for nonradiative losses	$10^{19}\mathrm{cm^{-3}}$
n_e^0	hole density for nonradiative losses	$10^{19}\mathrm{cm^{-3}}$

III. RESULTS

In this section results for an example structure with a single quantum well and a ridge width of $10\,\mu$m that exhibits multiple transverse modes are shown. The structure is described in more detail in Table II in the appendix. To calculate two-dimensional mode functions in (2) the dielectric function from [38] is used. Additionally the dielectric function of the quantum well is considered for a reference carrier density of $1 \times 10^{13}\,\mathrm{cm^{-2}}$. As mentioned before, the band structure of the quantum well is required to compute the optical properties such as the susceptibility. For this purpose the $\mathbf{k}\cdot\mathbf{p}$-Hamiltonian proposed by Chuang et al. is used [39], [40], [41], the method is described in more detail in [26]. The thickness of the InGaN quantum well used in the simulations is given by $2\,$nm, the indium concentration by $28\,\%$ and the material parameters are taken from [40]. The formulas for the susceptibility and the mode interaction term are given in the appendix.

For the charge carrier mobilities the model as described in [42] is used. The Drift-Diffusion equations are solved using the finite volume method with the Scharfetter-Gummel scheme for the carrier current densities [43]. The remaining simulation parameters for the simulations are shown in Table I.

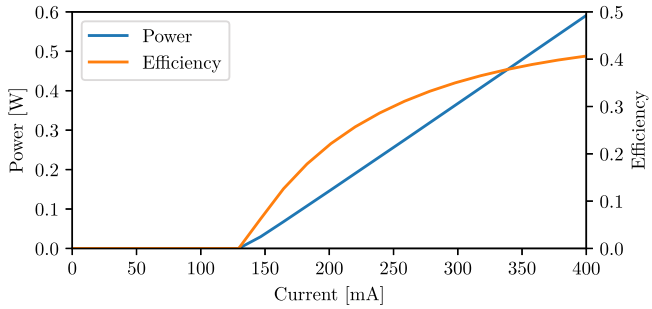

Fig. 2. Blue line shows the optical power as a function of the current for the steady state simulation. The efficiency is also shown as an orange line, which has been calculated by dividing the optical power by the electric power $I \cdot U$.

In Fig. 1 the current densities and the bulk carrier recombination are shown for a voltage above threshold. With the chosen parameters most of the carrier recombination is caused by the capture term at the position of the quantum well. The steady-state simulation also gives access to the photon numbers S_{mp}, which allows the calculation of the optical power

$$P = \sum_{mp} \hbar\omega_{mp} \frac{S_{mp}}{\tau_\mathrm{photon}},$$

which is shown in Fig. 2 as a function of the current I. This can be useful for the calculation of the threshold current and to choose the loss parameters in order to reproduce experimental results.

The corresponding pump current densities are shown in Fig. 3 for different voltages. Due to the low hole mobility the pump current densities are high below the ridge and small in the other regions, but as the n-contacts are on the sides and far away from the ridge, the pump current densities have a maximum near the

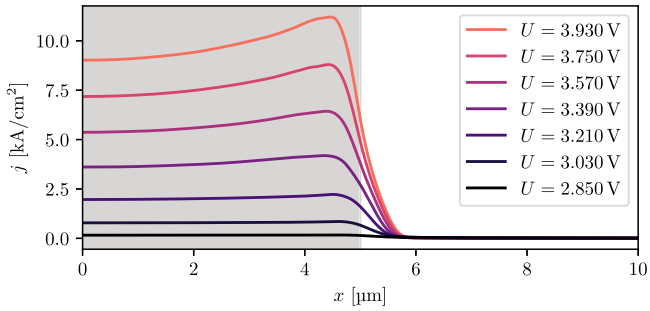

Fig. 3. Electron pump current densities from (9) for different voltages near the threshold. The hole pump current densities look almost identical. The grey area indicates the region below the ridge.

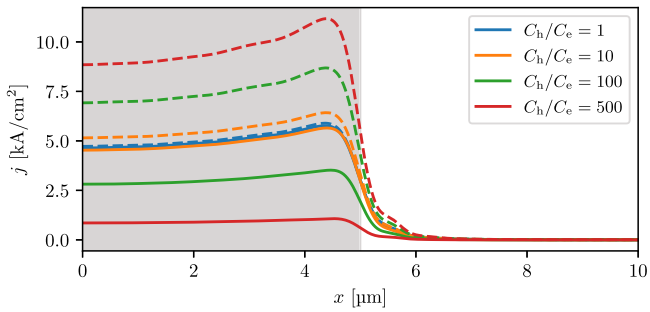

Fig. 4. Electron pump current densities from (9) for the structure with two quantum wells are shown for different ratios $C_\mathrm{h}/C_\mathrm{e}$ of the capture constants. The structure is the same as in Fig. 3 except for the additional QW, and is given in Table II in the appendix.

edge of the ridge. This maximum is more pronounced for larger voltages.

The method can also be used for structures with multiple quantum wells. In this case the pump current densities depend strongly on the capture coefficients, which is shown in Fig. 4 for a structure with two quantum wells. For equal capture constants the current densities are split equally between the quantum wells. However, due to the lower hole mobility the hole capture constant is expected to be larger. As expected this results in a higher pump current density for the quantum well on the p-side.

Using these results it is possible to perform a mode dynamics simulation, as shown in Fig. 5 for different currents. These simulations are carried out by solving the equations of motion (4) and (5), which yield the photon numbers S_{mp} over time. In addition the one-dimensional Eigen (7) is solved at every time step in to correct the mode profiles and to calculate the effective refractive index and the group refractive index. These refractive indices are then used in (3) to calculate the mode frequencies at every time step, which are shown in Fig. 6 as a function of time. At the beginning of the simulation they change due to changes of the carrier densities in the quantum well. However after the relaxation oscillations are finished, the mode wavelengths remain constant in time and the changes do not play a role for the simulation of the mode dynamics.

The simulated streak camera images of Fig. 5 are then obtained by performing a sum over all modes at every time step, where the contribution of each mode is given by Gaussian

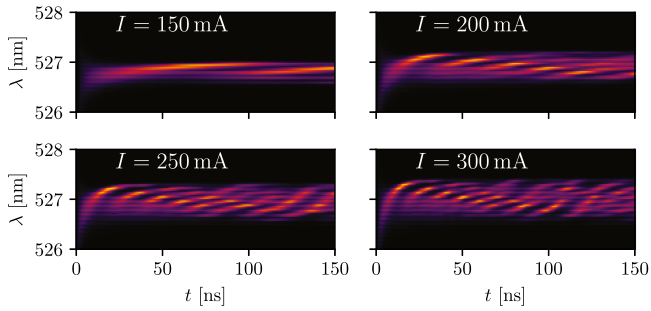

Fig. 5. Longitudinal and transverse mode dynamics of a Fabry-Pérot laser diode with a single quantum well for four different currents. Here the output of the laser is shown as a function of wavelength and time. The data for this figure is calculated by multiplying the time-dependent photon numbers from the simulation with Gaussian functions that are centered at their respective vacuum wavelengths with a width of $0.02\,\mathrm{nm}$.

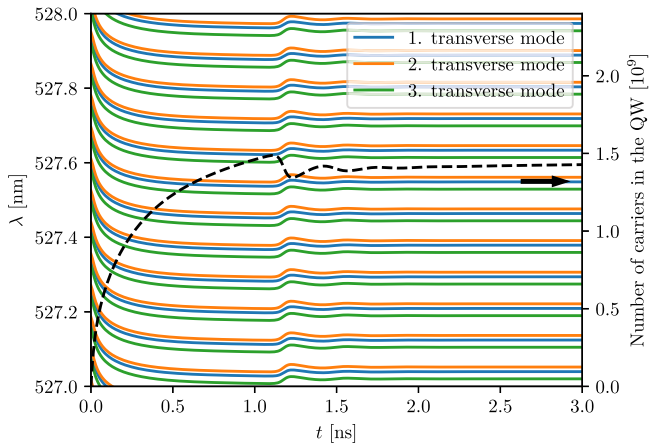

Fig. 6. Changes of the mode wavelengths over time for $I = 150\,\mathrm{mA}$ for the first three transverse modes. As the changes of the mode wavelengths are caused by changes of the quantum well refractive index, the quantum well carrier number is also shown as a dashed line. The carrier number was calculated by integrating both the hole and the electron densities over the quantum well area.

function centered at the respective vacuum wavelength and an amplitude given by the photon number. The effect of mode hopping can be observed, where the laser output wavelength periodically changes from lower to higher values. As multiple transverse modes participate, the contributions of the respective longitudinal modes overlap, making it difficult to identify individual modes. This has been also observed experimentally for laser diodes with an even broader ridge of $40\,\mu\mathrm{m}$ [10]. However the overall mode dynamics are very similar to As the effect of mode hopping is observable for small ridge laser diodes and can be explained by an interaction of the longitudinal modes, the coupling between different transverse modes does not seem to be as significant. This can be explained by the integral for the mode interaction in (6), which is larger for two modes with the same transverse mode profile, as the overlap of the respective absolute squares is is increased.

To investigate this further, it can be of interest to look at the contributions of different transverse modes separately, which is shown in Fig. 7. In this case the different longitudinal modes

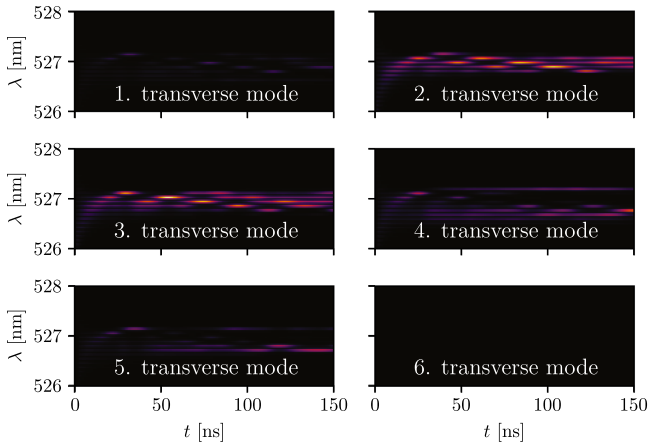

Fig. 7. Contributions of different transverse modes to the mode dynamics for a laser diode with a single quantum well and a current of 200 mA.

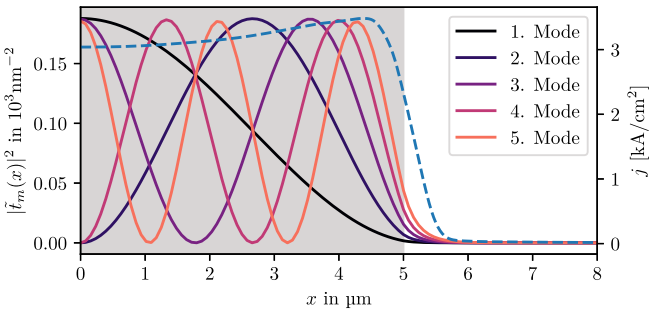

Fig. 8. First five transverse mode functions at the position of the quantum well are shown as a function of the lateral coordinate x. Additionally the electron pump current density for a current of 200 mA is shown as a blue dashed line.

can be observed, and the frequency separation $\Delta\omega = \frac{\pi c}{L n_{\mathrm{gr}}}$ is determined by the cavity length L. For the considered structure the fundamental mode is not active, because the pump current maximum is not in the middle of the structure but near the edge of the ridge, as illustrated in Fig. 8, where the transverse mode functions at the position of the quantum well are shown together with pump current density for a current of 200 mA. If the current is increased further, more transverse modes will participate due to spatial hole burning.

IV. Summary

In this publication a model for the simulation of mode dynamics in Fabry-Pérot type laser diodes with larger ridge widths and multiple lateral modes is presented. The carrier transport from the contacts to the active region is calculated for the steady state using the Drift-Diffusion model. The carriers in the quantum well are treated separately and are connected to bulk carriers using a capture term. The interaction between two different modes can de derived from third-order effects and is described in the simulation by an effective interaction term. This term strongly depends on the difference of the mode frequencies and the quantum well carrier densities.

Simulation results are shown for a green nitride laser diode with a ridge width of 10 µm, but in principle this model can be used for other materials and geometries. The effect of mode hopping can be observed in the resulting mode dynamics, which can also observed experimentally for similar structures [10]. However, the experiments show multiple mode clusters. In order to obtain the same behavior in simulations the presented model could be extended, for example fluctuations of the indium content in the quantum wells can be taken into account in future work.

Appendix

A. Calculation of the Susceptibility and the Mode Interaction

For the calculation of the susceptibility and the mode interaction the same formulas as in [26] are used. In order to keep the calculations simple for the example structure, a constant scattering time τ_s is used to describe the carrier scattering. It is of course possible to use more complicated scattering terms as described in [26] in more detail. Similarly a dephasing constant γ is used to describe the homogenous broadening and Hartree-Fock corrections are neglected. In this case the susceptibility is given by

$$\chi(\omega) = \frac{2}{A}\sum_{\lambda\mathbf{k}} \frac{e^2|p_\lambda|^2}{\epsilon_0 m_0^2\omega^2}\frac{1-f^{\mathrm{e}}_{\mathbf{k}}-f^{\lambda}_{\mathbf{k}}}{\hbar\omega+i\gamma-\varepsilon^{\mathrm{e}}_{\mathbf{k}}-\varepsilon^{\lambda}_{\mathbf{k}}}.$$

Here λ is used as index for the hole bands and the carrier distributions are given by Fermi-Dirac distributions for a given temperature and carrier densities. The quantum well band structure $\varepsilon^{\lambda}_{\mathbf{k}}$ and momentum matrix elements p_λ are calculated using the $\mathbf{k}\cdot\mathbf{p}$ method. The mode interaction in (6) can be split into symmetric and antisymmetric contributions with respect to the frequency difference of the two modes $\Delta\omega$:

$$G(\Delta\omega) = G_{\mathrm{S}}(\Delta\omega) + G_{\mathrm{A}}(\Delta\omega). \tag{10}$$

For a constant scattering time the symmetric mode interaction strength is given by

$$\begin{aligned} G_{\mathrm{S}}(\Delta\omega) &= \omega_0^4 \mathrm{Im}\,\chi(\omega_0)\mathrm{Im}\,\chi'(\omega_0)\frac{\tau_{\mathrm{s}}}{\Delta\omega^2\tau_{\mathrm{s}}^2+1} \\ &\quad -\sum_{\lambda\lambda'\mathbf{k}}\frac{e^4|p_\lambda|^2|p_{\lambda'}|^2}{m_0^4\epsilon_0^2}\frac{\tau_{\mathrm{s}}(1+\delta_{\lambda\lambda'})}{\Delta\omega^2\tau_{\mathrm{s}}^2+1} \\ &\quad \times\frac{2}{A}\frac{\gamma^2(1-f^{\mathrm{e}}_{\mathbf{k}}-f^{\lambda'}_{\mathbf{k}})}{\left((\hbar\omega_0-\varepsilon^{\mathrm{e}}_{\mathbf{k}}-\varepsilon^{\lambda}_{\mathbf{k}})^2+\gamma^2\right)\left((\hbar\omega_0-\varepsilon^{\mathrm{e}}_{\mathbf{k}}-\varepsilon^{\lambda'}_{\mathbf{k}})^2+\gamma^2\right)} \end{aligned}$$

and the antisymmetric interaction term is given by

$$G_{\mathrm{A}}(\Delta\omega) = \omega_0^4\frac{\mathrm{Im}\,\chi(\omega_0)\mathrm{Re}\,\chi'(\omega_0)}{\Delta\omega}.$$

The mode interaction term is shown in Fig. 9 for the parameters used in the simulations and different carrier densities.

The carrier losses in the quantum well due to spontaneous emission are given by [26], [44]

$$B(n_{\mathrm{e}},n_{\mathrm{h}}) = \frac{2}{A}\sum_{\lambda\mathbf{k}}\frac{2e^2|p_\lambda|^2 n_{\mathrm{eff}}^3}{3\pi m_0^2\epsilon_0 c^3\hbar^2}\left(\varepsilon^{\mathrm{e}}_{\mathbf{k}}+\varepsilon^{\lambda}_{\mathbf{k}}\right)f^{\mathrm{e}}_{\mathbf{k}}f^{\lambda}_{\mathbf{k}}.$$

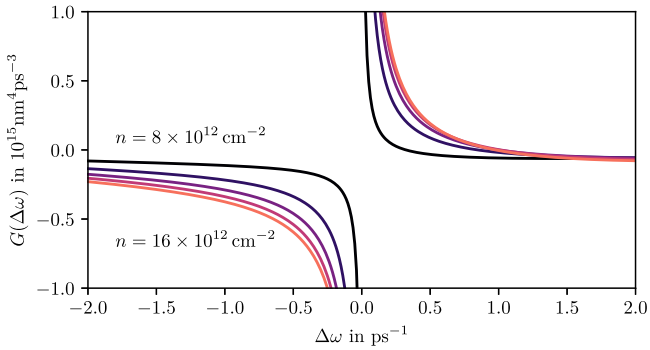

Fig. 9. Mode interaction strength from (10) as a function of the frequency difference $\Delta\omega$ for different carrier densities.

TABLE II
STRUCTURAL PARAMETERS FOR THE LASER DIODE USED IN THE CALCULATIONS, ADAPTED FROM [45]

Thickness	Width	Material	Doping
55 nm	10 µm	GaN	$1 \times 10^{18}\,\mathrm{cm^{-2}}$
340 nm	10 µm	$Al_{0.08}Ga_{0.92}N$	$1 \times 10^{18}\,\mathrm{cm^{-2}}$
10 nm	30 µm	$Al_{0.15}Ga_{0.85}N$	$1 \times 10^{18}\,\mathrm{cm^{-2}}$
15 nm	30 µm	GaN	$1 \times 10^{18}\,\mathrm{cm^{-2}}$
50 nm	30 µm	GaN	$0\,\mathrm{cm^{-2}}$
13 nm	30 µm	$In_{0.05}Ga_{0.95}N$	$0\,\mathrm{cm^{-2}}$
2 nm	30 µm	$In_{0.22}Ga_{0.78}N$	$0\,\mathrm{cm^{-2}}$
8 nm	30 µm	$In_{0.05}Ga_{0.95}N$	$0\,\mathrm{cm^{-2}}$
2 nm	30 µm	$In_{0.22}Ga_{0.78}N$	$0\,\mathrm{cm^{-2}}$
13 nm	30 µm	$In_{0.05}Ga_{0.95}N$	$0\,\mathrm{cm^{-2}}$
115 nm	30 µm	GaN	$-1 \times 10^{18}\,\mathrm{cm^{-2}}$
1300 nm	30 µm	$Al_{0.06}Ga_{0.94}N$	$-1 \times 10^{18}\,\mathrm{cm^{-2}}$
4000 nm	50 µm	GaN	$-1 \times 10^{18}\,\mathrm{cm^{-2}}$

The spontaneous emission spectrum I_{SE} in (5) is calculated like the susceptibility, except that the factor $1 - f^{\mathrm{e}}_{\mathbf{k}} - f^{\lambda}_{\mathbf{k}}$ is replaced by $f^{\mathrm{e}}_{\mathbf{k}} f^{\lambda}_{\mathbf{k}}$:

$$I_{\mathrm{SE}}(\omega) = -\frac{2}{A} \sum_{\lambda \mathbf{k}} \frac{e^2 |p_\lambda|^2}{m_0^2 \epsilon_0 \omega} \mathrm{Im} \left\{ \frac{f^{\mathrm{e}}_{\mathbf{k}} f^{\lambda}_{\mathbf{k}}}{\hbar\omega + i\gamma - \varepsilon^{\mathrm{e}}_{\mathbf{k}} - \varepsilon^{\lambda}_{\mathbf{k}}} \right\}.$$

B. Structural Parameters

The example structure with one quantum well used in the simulations has been obtained by stretching the structure in [45] in lateral direction. The structural parameters are given in Table II. The example structure with two quantum wells is obtained by repeating the 2 nm and 8 nm layers. The p-contact is located on top of the ridge and the n-contact is on top of the substrate with a distance of 10 μm to the diode.

REFERENCES

[1] L. Jiang et al., "GaN-based green laser diodes," *J. Semicond.*, vol. 37, no. 11, 2016, Art. no. 111001, doi: 10.1088/1674-4926/37/11/111001.

[2] Y. Nakatsu et al., "High-efficiency blue and green laser diodes for laser displays," *Proc. SPIE*, vol. 10918, pp. 99–107, 2019.

[3] N. Shimada, M. Yukawa, K. Shibata, K. Ono, T. Yagi, and A. Shima, "640-nm laser diode for small laser display," *Proc. SPIE*, vol. 7198, pp. 46–53, 2009. [Online]. Available: https://www.scopus.com/inward/record.uri?eid=2-s2.0-65649111283&doi=10.1117%2f12.808710&partnerID=40&md5=7bac3d51a64e6d3fffce94ba8760e91f

[4] S. Masui, T. Miyoshi, T. Yanamoto, and S.-I. Nagahama, "Blue and green laser diodes for large laser display," in *Proc. IEEE Conf. Lasers Electro-Opt. Pacific Rim*, 2013, pp. 1–2. [Online]. Available: https://www.scopus.com/inward/record.uri?eid=2-s2.0-84885440678&doi=10.1109%2fCLEOPR2013.6599913&partnerID=40&md5=c7a1857bfe2377ff19b1023d245751d6

[5] D. Queren et al., "500 nm electrically driven InGaN based laser diodes," *Appl. Phys. Lett.*, vol. 94, no. 8, 2009, Art. no. 081119, doi: 10.1063/1.3089573.

[6] S. Lutgen et al., "Recent results of blue and green InGaN laser diodes for laser projection," *Proc. SPIE*, vol. 7953, pp. 108–119, 2011. [Online]. Available: https://www.scopus.com/inward/record.uri?eid=2-s2.0-79953125633&doi=10.1117%2f12.874757&partnerID=40&md5=3be51cbc620eb47e303967f9af2c550f

[7] J. Raring et al., "47.1: Invited paper: Progress in green and blue laser diodes and their application in pico projection systems," *Dig. Tech. Papers - SID Int. Symp.*, vol. 42, no. 1, pp. 677–680, 2011. [Online]. Available: https://www.scopus.com/inward/record.uri?eid=2-s2.0-84863228582&doi=10.1889%2f1.3621414&partnerID=40&md5=82d36f241d61015bfa830bb805cedab4

[8] T. Weig, T. Hager, G. Brüderl, U. Strauss, and U. T. Schwarz, "Longitudinal mode competition and mode clustering in (Al,In)GaN laser diodes," *Opt. Exp.*, vol. 22, no. 22, 2014, Art. no. 27489.

[9] E. Kuhn, L. Uhlig, M. Wachs, U. Schwarz, and A. Thränhardt, "Mode rolling effects in nitride laser diodes," *Eng. Res. Exp.*, vol. 2, no. 3, 2020, Art. no. 035036. [Online]. Available: https://www.scopus.com/inward/record.uri?eid=2-s2.0-85092582861&doi=10.1088%2f2631-8695%2fabb6c8&partnerID=40&md5=ac606f6679bf8bc9942faf9dca16c33f

[10] L. Uhlig, D. J. Kunzmann, and U. T. Schwarz, "Characterization of lateral and longitudinal mode competition in blue InGaN broad-ridge laser diodes," *Physica Status Solidi (a)*, vol. 220, no. 16, 2023, Art. no. 2200751. [Online]. Available: https://onlinelibrary.wiley.com/doi/abs/10.1002/pssa.202200751

[11] M. Yamada, "Theoretical analysis of nonlinear optical phenomena taking into account the beating vibration of the electron density in semiconductor lasers," *J. Appl. Phys.*, vol. 66, no. 1, pp. 81–89, Nov. 1989.

[12] G. Agrawal and N. Olsson, "Self-phase modulation and spectral broadening of optical pulses in semiconductor laser amplifiers," *IEEE J. Quantum Electron.*, vol. 25, no. 11, pp. 2297–2306, Nov. 1989.

[13] S. Balsamo, F. Sartori, and I. Montrosset, "Dynamic beam propagation method for flared semiconductor power amplifiers," *IEEE J. Sel. Topics Quantum Electron.*, vol. 2, no. 2, pp. 378–384, Jun. 1996.

[14] C. Z. Ning, R. A. Indik, and J. V. Moloney, "Effective Bloch equations for semiconductor lasers and amplifiers," *IEEE J. Quantum Electron.*, vol. 33, no. 9, pp. 1543–1550, Sep. 1997.

[15] U. Bandelow, M. Radziunas, J. Sieber, and M. Wolfrum, "Impact of gain dispersion on the spatio-temporal dynamics of multisection lasers," *IEEE J. Quantum Electron.*, vol. 37, no. 2, pp. 183–188, Feb. 2001.

[16] R. Čiegis and M. Radziunas, "Effective numerical integration of traveling wave model for edge-emitting broad-area semiconductor lasers and amplifiers," *Math. Modelling And Anal.*, vol. 15, pp. 409–430, 2010.

[17] M. Radziunas, "Modeling and simulations of edge-emitting broad-area semiconductor lasers and amplifiers," in *Proc. Parallel Process. Appl. Math.*, 2016, pp. 269–276.

[18] M. Radziunas, "Modeling and simulations of broad-area edge-emitting semiconductor devices," *Int. J. High Perform. Comput. Appl.*, vol. 32, no. 4, pp. 512–522, 2018.

[19] E. Kuhn and A. Thränhardt, "Modeling mode competition in laser diodes," *Opt. Quantum Electron.*, vol. 51, no. 6, pp. 1–12, 2019. [Online]. Available: https://www.scopus.com/inward/record.uri?eid=2-s2.0-85067930093&doi=10.1007%2fs11082-019-1916-7&partnerID=40&md5=07da018e859db7d0cc7802f3ecf6a339

[20] W. E. Lamb, "Theory of an optical maser," *Phys. Rev.*, vol. 134, pp. A1429–A1450, Jun. 1964, doi: 10.1103/PhysRev.134.A1429.

[21] M. Yamada, "Transverse and longitudinal mode control in semiconductor injection lasers," *IEEE J. Quantum Electron.*, vol. 19, no. 9, pp. 1365–1380, Sep. 1983.

[22] M. Yamada, "Theory of mode competition noise in semiconductor injection lasers," *IEEE J. Quantum Electron.*, vol. 22, no. 7, pp. 1052–1059, Jul. 1986.

[23] M. Ahmed, M. Yamada, and M. Saito, "Numerical modeling of intensity and phase noise in semiconductor lasers," *IEEE J. Quantum Electron.*, vol. 37, no. 12, pp. 1600–1610, Dec. 2001.

[24] M. Ahmed and M. Yamada, "Influence of instantaneous mode competition on the dynamics of semiconductor lasers," *IEEE J. Quantum Electron.*, vol. 38, no. 6, pp. 682–693, Jun. 2002.

[25] M. Ahmed, "Theoretical modeling of intensity noise in InGaN-semiconductor lasers," *Sci. World J.*, vol. 2014, 2014, Art. no. 475423.

[26] E. Kuhn and A. Thränhardt, "Influence of scattering effects on the interaction between longitudinal modes in laser diodes," *Phys. Rev. B*, vol. 108, Sep. 2023, Art. no. 115304, doi: 10.1103/PhysRevB.108.115304.

[27] T. Koprucki and K. Gärtner, "Discretization scheme for drift-diffusion equations with strong diffusion enhancement," *Opt. Quantum Electron.*, vol. 45, no. 7, pp. 791–796, 2013. [Online]. Available: https://www.scopus.com/inward/record.uri?eid=2-s2.0-84880035136&doi=10.1007%2fs11082-013-9673-5&partnerID=40&md5=1183f5560accf09b9f5fb45c94c58e8a

[28] T. Koprucki, N. Rotundo, P. Farrell, D. Doan, and J. Fuhrmann, "On thermodynamic consistency of a scharfetter–gummel scheme based on a modified thermal voltage for drift-diffusion equations with diffusion enhancement," *Opt. Quantum Electron.*, vol. 47, no. 6, pp. 1327–1332, 2015. [Online]. Available: https://www.scopus.com/inward/record.uri?eid=2-s2.0-84930088463&doi=10.1007%2fs11082-014-0050-9&partnerID=40&md5=a904f5f36e8e35c35efbed3e0a8a2bcb

[29] H. Gajewski, M. Liero, R. Nürnberg, and H. Stephan, "WIAS-TeSCA-two-dimensional semi-conductor analysis package," Weierstraß-Institut für Angewandte Analysis und Stochastik, Berlin, Germany, Tech. Rep. 14, 2016.

[30] R. Sarzała et al., "Numerical self-consistent analysis of vcsels," *Adv. Opt. Technol.*, vol. 2012, May 2012, Art. no. 689519, doi: 10.1155/2012/689519.

[31] A. Tibaldi, F. Bertazzi, M. Goano, R. Michalzik, and P. Debernardi, "VENUS: A vertical-cavity surface-emitting laser electro-opto-thermal numerical simulator," *IEEE J. Sel. Topics Quantum Electron.*, vol. 25, no. 6, Nov./Dec. 2019, Art. no. 1500212. [Online]. Available: https://www.scopus.com/inward/record.uri?eid=2-s2.0-85061931071&doi=10.1109%2fJSTQE.2019.2893755&partnerID=40&md5=5b537e965c7ff8e1b2f254d93deff3ff

[32] S. Chuang, *Physics of Optoelectronic Devices* (Wiley Series in Pure and Applied Optics). Hoboken, NJ, USA: Wiley, 1995. [Online]. Available: https://books.google.de/books?id=ect6QgAACAAJ

[33] M. Kira and S. W. Koch, *Semiconductor Quantum Optics*. Cambridge, U.K.: Cambridge Univ. Press, 2011.

[34] J. Buus, "Models of the static and dynamic behavior of stripe geometry lasers," *IEEE J. Quantum Electron.*, vol. 19, no. 6, pp. 953–960, Jun. 1983.

[35] J. Piprek, *Handbook of Optoelectronic Device Modeling and Simulation: Lasers, Modulators, Photodetectors, Solar Cells and Numerical Methods* (Series in Optics and Optoelectronics), vol. 2. Boca Raton, FL, USA: CRC Press, 2017. [Online]. Available: https://books.google.de/books?id=MGpQDwAAQBAJ

[36] S. M. Sze and K. K. Ng, *Physics and Properties of Semiconductors–A Review*. Hoboken, NJ, USA: Wiley, 2006, doi: 10.1002/9780470068328.ch1.

[37] A. Tibaldi et al., "Bridging scales in multiphysics VCSEL modeling," *Opt. Quantum Electron.*, vol. 51, no. 7, pp. 1–19, 2019. [Online]. Available: https://www.scopus.com/inward/record.uri?eid=2-s2.0-85067988772&doi=10.1007%2fs11082-019-1931-8&partnerID=40&md5=6ac2b1ee4d057ebe520a6a352e2d8b0b

[38] R. Goldhahn, C. Buchheim, P. Schley, A. T. Winzer, and H. Wenzel, "Optical Constants of Bulk Nitrides," in *Nitride Semiconductor Devices: Principles and Simulation*. Hoboken, NJ, USA: Wiley, 2007, ch. 5, pp. 95–115, doi: 10.1002/9783527610723.ch5.

[39] S. L. Chuang and C. S. Chang, "A band-structure model of strained quantum-well wurtzite semiconductors," *Semicond. Sci. Technol.*, vol. 12, no. 3, pp. 252–263, 1997.

[40] J. Piprek, *Nitride Semiconductor Devices: Principles and Simulation*. Hoboken, NJ, USA: Wiley, 2007.

[41] T. R. Nielsen, P. Gartner, M. Lorke, J. Seebeck, and F. Jahnke, "Coulomb scattering in nitride-based self-assembled quantum dot systems," *Phys. Rev. B.- Condens. Matter Mater. Phys.*, vol. 72, no. 23, 2005, Art. no. 235311. [Online]. Available: https://www.scopus.com/inward/record.uri?eid=2-s2.0-29744442906&doi=10.1103%2fPhysRevB.72.235311&partnerID=40&md5=42b902f6247bfb95097631b7b2eacc5b

[42] T. T. Mnatsakanov, M. E. Levinshtein, L. I. Pomortseva, S. N. Yurkov, G. S. Simin, and M. A. Khan, "Carrier mobility model for GaN," *Solid-State Electron.*, vol. 47, no. 1, pp. 111–115, 2003. [Online]. Available: https://www.sciencedirect.com/science/article/pii/S0038110102002563

[43] D. Scharfetter and H. Gummel, "Large-signal analysis of a silicon read diode oscillator," *IEEE Trans. Electron Devices*, vol. 16, no. 1, pp. 64–77, Jan. 1969.

[44] O. Hess and T. Kuhn, "Maxwell-Bloch equations for spatially inhomogeneous semiconductor lasers. I. theoretical formulation," *Phys. Rev. A*, vol. 54, no. 4, pp. 3347–3359, 1996.

[45] T. Weig, "Generation of optical ultra–short pulses in (AL, In) GaN laser diodes," Doctoral Dissertation, Albert-Ludwigs-Universität Freiburg, Breisgau, Germany, 2015.